Topological Similarity of Sponge-like Bicontinuous Morphologies Differing in Length Scale**

By *Hiroshi Jinnai*, *Yukihiro Nishikawa*, *Masako Ito*, *Steven D. Smith*, *David A. Agard*, and *Richard J. Spontak**

Bicontinuous morphologies form spontaneously in physical and biological systems,[1–3] and are of increasing scientific and technological interest.[4] Recent studies of bicontinuous polymer systems have elucidated[5] the molecular factors responsible for the stability of such complex morphologies, and have established[6,7] the utility of these morphologies as templating media by which to produce nanoporous materials for separations, microelectronics, and catalysis. While some bicontinuous morphologies exhibit long-range order and can be categorized according to spatial symmetry, others do not. We refer to the latter as *sponge-like*. Investigation of spatially complex morphologies requires local and global structural information derived from direct 3D visualization for the purposes of improved understanding, accurate classification, and rational design. By analyzing 3D images, we demonstrate that the local and topological features of sponge-like morphologies in vastly different systems—synthetic polymers and trabecular bone—are remarkably similar. Since these morphologies span about four orders of magnitude in size, our results not only provide unprecedented evidence for size-independent structural similarity, but should also i) facilitate the design of (bio)materials with tailored bicontinuous morphologies, and ii) provide greater insight into the function of sponge-like morphologies encountered in materials and medical science.

Cubic bicontinuous morphologies, composed of non-intersecting channel networks, are ubiquitous in soft, self-organized systems composed of low-molar-mass (bio)surfactant molecules.[1,3] Several ordered bicontinuous morphologies are known to exist in such systems, but only one, the bicontinuous L_3 morphology, is considered further here as an example of an aperiodic sponge-like nanostructure. This particular morphology consists of randomly connected membranes and appears[8,9] as swollen, defect-riddled mono- or bilayers. Block copolymers behave[10] as macromolecular surfactants, and likewise exhibit[11,12] both ordered and sponge-like bicontinuous nanostructures at larger, more experimentally accessible length scales, typically measuring tens of nanometers. While spatially ordered bicontinuous morphologies such as the gyroid[5,13–15] ($Ia\bar{3}d$ symmetry), perforated lamellae[16] ($P6_3/mmc$ symmetry), and "Plumber's Nightmare"[7] ($Im\bar{3}m$ symmetry) have been the subject of most contemporary studies, sponge-like bicontinuous morphologies have been observed in binary[12,17,18] and ternary[19] block copolymer systems.

Since bicontinuous nanostructures continue to gain widespread attention as, for example, precursors for nano- and mesoporous materials in separation, microelectronic, and catalysis technologies,[6,7,20] accurate structural analysis and classification are critical prerequisites for rational design. Characterization of highly ordered bicontinuous morphologies in surfactant and polymer systems has traditionally relied on crystallographic analysis[6,13–15] and minimal-surface models.[21] While these approaches are useful for analyzing ordered systems, direct 3D visualization of spatially complex morphologies by real-space imaging methods, such as transmission electron microtomography (TEMT) or, at larger length scales, laser scanning confocal microscopy (LSCM) and X-ray microcomputed tomography (μCT), is required for model-independent analysis. Of particular interest has been the development[22,23] of classification paradigms based on local and global topological characteristics. Local topology is expressed in terms of mean (H) and Gaussian (K) interfacial curvatures that together reflect the shape of the interface and, hence, its molecular packing frustration[5] and elastic bending energy[24] (f), expressed as $f = \int(2\kappa H^2 + \kappa' K)\mathrm{d}A$, where κ and κ' denote the bending rigidity and splay modulus, respectively, and A represents interfacial area. Global topological metrics, such as the coordination (N_c) and Euler–Poincaré characteristic (χ), provide insight into structural connectivity and constitute established[2,25] methods by which to compare complex curved surfaces in quantitative fashion.

These non-parametric classification paradigms are completely general and are especially well-suited to the quantitative analysis of bicontinuous morphologies exhibiting no long-range order, such as the sponge nanostructure in surfactant and block copolymer systems. Another pertinent example is the sponge-like microstructure that develops during the spinodal decomposition (SD) of a polymer blend.[26] In this work, we seek to discern the extent to which sponge-like systems of vastly different size scales exhibit similar bicontinuous morphologies. This is best achieved by analyzing and comparing the topological features of a block copolymer (BC) blend (nanometer scale), and two SD polymer blends (micrometer scale), which are all synthetic materials, as well as trabecular bone (TB), which is a naturally occurring biological system that exhibits sponge-like bicontinuity at the millimeter scale.

[*] Prof. R. J. Spontak
Departments of Chemical Engineering and Materials Science & Engineering, North Carolina State University
Raleigh, NC 27695 (USA)
E-mail: Rich_Spontak@ncsu.edu

Dr. H. Jinnai, Dr. Y. Nishikawa
Department of Polymer Science & Engineering
Kyoto Institute of Technology
Kyoto 606-8585 (Japan)

Dr. M. Ito
Department of Radiology, Nagasaki University School of Medicine
Nagasaki 852-8521 (Japan)

Dr. S. D. Smith
Corporate Research Division, The Procter & Gamble Company
Cincinnati, OH 45239 (USA)

Prof. D. A. Agard
Departments of Biochemistry & Biophysics and Howard Hughes Medical Institute, University of California
San Francisco, CA 94143 (USA)

[**] This study was supported by the Ministry of Education, Science, Sports and Culture of Japan (H.J.), the Research Society for Metabolic Bone Diseases (M.I.), the National Institutes of Health (D.A.A.), the U.S. Department of Energy under Contract No. DE-FG02-99ER14991, and the NC State University Office of International Programs (R.J.S.).

  0935-9648/02/2211-1615 $ 17.50+.50/0

ADVANCED MATERIALS

While other examples of sponge-like bicontinuous morphologies exist in nature,[2] we include bone due to challenges regarding structural degeneration (e.g., osteoporosis) that persist in biomedical research, and ongoing interest in developing bone-like materials for graft and regenerative purposes.

Figure 1 provides cut-away views of four of the 3D images analyzed during the course of this study. Volumetric images of these specimens, designated and described in the caption of Figure 1, have been acquired by either TEMT,[15,18] LSCM,[26] or μCT,[27] and subsequently subjected to a series of image-processing algorithms[23,24] to generate accurate representations of the interfaces residing therein. Included in this figure are the corresponding correlation lengths (L), each measured from the position of the intensity maximum in the calculated structure factor. Measured values of L, determined from Fourier analysis, range from 90 nm to 0.82 mm (depicted in Fig. 1 and listed in Table 1), indicating that these morphologies span about four orders of magnitude in size. Cursory examination of the images displayed in Figure 1 reveals that, despite their substantial difference in size, these sponge-like morphologies appear qualitatively similar.

The mean and Gaussian curvatures at any point on an interface describe the local interfacial shape, which can impact mechanical performance.[28] These curvatures are expressed in terms of the principal radii of curvature r_1 and r_2 defined by the two tangential circles illustrated in Figure 2. The probability densities of these curvatures—$P_H(H)$ and $P_K(K)$, respectively—are derived from a joint interfacial curvature probability distribution, determined by measuring H and K at random points along the interface.[22,26] Since previous theoretical studies[5] have shown that P_H governs the thermodynamic stability of bicontinuous nanostructures in polymer systems, Figure 3 displays P_H for the BC blend (Fig. 3a), two SD blends (Fig. 3b), and three TB specimens (Fig. 3c). These probability distributions exhibit two important characteristics. The first is their overall shape, which consistently appears Gaussian, and the second is their average. Area-averaged mean curvatures ($\langle H \rangle$) and their corresponding standard deviations (σ_H), ascertained from Figure 3, are included in Table 1 and reveal that several, but not all, of the morphologies exhibit $\langle H \rangle \approx 0$ (in appropriate units), which is prerequisite for a minimal surface.[2,21] While recent results have demonstrated[29] that $\langle H \rangle$ correlates with the structure model index (SMI) developed to describe bone microstructure, the present work shows that the probability densities P_H and P_K, and not just average quantities, must be considered in

Table 1. Interfacial curvature and topological characteristics of sponge-like bicontinuous morphologies.

	Block copolymer	SD polymer blends		Trabecular bone		
Property	BC	SD_1	SD_2	TB_1	TB_2	TB_3
L [mm]	89.6×10^{-6}	20.4×10^{-3}	11.5×10^{-3}	0.496	0.780	0.820
$\lvert\langle H\rangle\rvert$ [mm^{-1}]	1.32×10^{3}	4.91×10^{1}	1.28×10^{1}	1.07	9.00×10^{-3}	6.91×10^{-1}
σ_H [mm^{-1}]	3.44×10^{4}	1.07×10^{2}	1.43×10^{2}	2.35	2.60	4.30
$\lvert\langle\tilde{H}\rangle\rvert$	3.96×10^{-2}	3.27×10^{-1}	5.74×10^{-2}	3.43×10^{-1}	3.72×10^{-3}	2.94×10^{-1}
Σ [mm^{-1}]	3.33×10^{4}	1.50×10^{2}	2.23×10^{2}	3.12	2.42	2.35
N_c [%]						
3	88.6	86.1	83.5	89.8	82.4	85.0
4	8.0	11.0	14.3	9.5	9.8	10.0
5	2.9	1.6	2.0	0.0	2.0	2.5
>5	0.5	1.3	0.2	0.7	5.8	2.5
n_j	1.90	1.98	2.29	1.76	0.93	1.02
χ [a]	–2.20	–2.48	–2.73	–0.489	–1.26	–1.23
χ_{GB} [b]	–3.36	–4.27	–4.17	–0.647	–0.545	–2.65
g [a]	2.10	2.24	2.36	1.28	1.63	1.65
g_{GB} [b]	2.68	3.14	3.09	1.32	1.27	2.32

[a] The Euler–Poincaré characteristic (χ), a measure of surface complexity, is determined from the total number of junctions (N_j) and branches (N_b) within each reconstructed image by $\chi = 2N_j - N_b$ and is related to the genus (g) by $\chi = 2(1-g)$. A surface of genus g is considered topologically equivalent to a sphere with g handles. [b] Estimated from the Gauss–Bonnet (GB) theorem, which states that χ is given by $(1/2\pi)\int K dA$ for a closed surface.

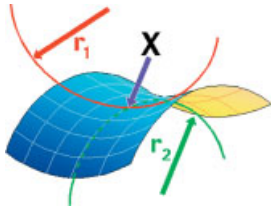

Fig. 2. A schematic diagram of a saddle-shaped interface showing the two tangential circles used to define the principal radii of curvature r_1 and r_2 at any point X on the interface. The mean (H) and Gaussian (K) curvatures at X are given by $(1/r_1+1/r_2)/2$ and $1/(r_1r_2)$, respectively.

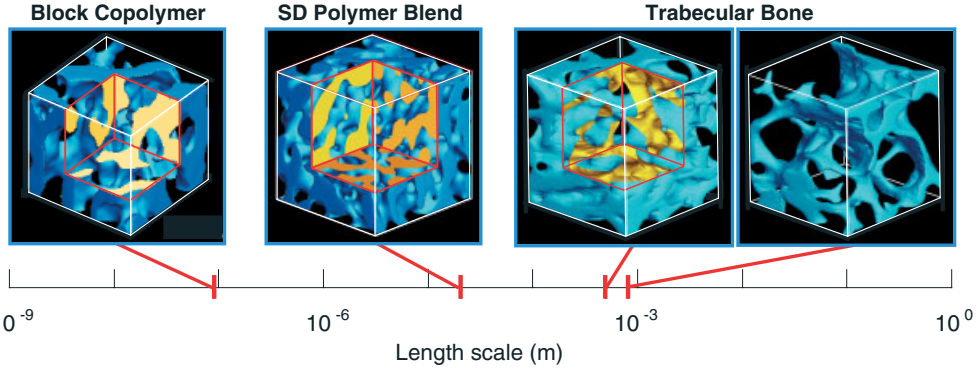

Fig. 1. Three-dimensional images of sponge-like bicontinuous morphologies formed in a block copolymer (BC) blend, a polymer blend (SD_1) undergoing late-stage spinodal decomposition and two examples of trabecular bone exhibiting layered (TB_1) and strut-like (TB_3) morphologies. The graduated length scale included in this figure displays the measured correlation length (L) of these morphologies for comparative purposes. Values of L are listed in Table 1.

  0935-9648/02/2211-1616 $ 17.50+.50/0 *Adv. Mater.* **2002**, *14*, No. 22, November 18

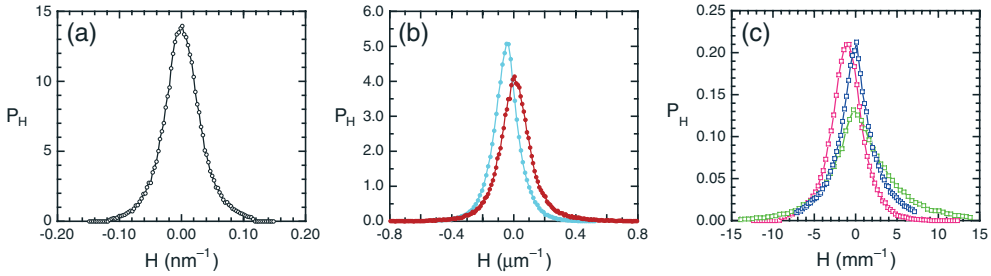

Fig. 3. Probability densities of the mean (H) curvature measured from sponge-like bicontinuous morphologies observed in a) a BC blend (open black circle), b) two SD polymer blends (SD_1 filled light blue circle, SD_2 filled red circle), and c) three TB specimens (TB_1 open green square, TB_2 open dark blue square, TB_3 open magenta square). The solid lines serve to connect the data.

discerning the extent to which diverse sponge-like nano- or microstructures are similar.

Since the morphologies examined here differ considerably in size, their interfacial curvature probability densities must be scaled with respect to the interfacial area/volume (Σ) for direct comparison.[23] This is achieved by introducing the dimensionless probability densities, $\tilde{P}_H(\tilde{H})$ and $\tilde{P}_K(\tilde{K})$, which are presented in Figures 4a and 4b, respectively. While $\tilde{P}_H$ derived from the BC blend, the symmetric SD_2 polymer blend and the TB_1 and TB_2 bone specimens in Figure 4a exhibit comparable broad maxima centered at $\tilde{H} \approx 0$, the $\tilde{P}_H$ corresponding to the compositionally asymmetric SD_1 polymer blend and the TB_3 bone specimen are virtually superimposed at $\tilde{H}_H < 0$. This result agrees well with that from the equally asymmetric gyroid morphology.[23] According to the data displayed in Figure 4b, most of $\tilde{P}_K$ for each morphology lies at $\tilde{K} < 0$, confirming that these interfaces are principally saddle-shaped (hyperbolic), as depicted in Figure 2. The $\tilde{P}_H$ and $\tilde{P}_K$ data presented in Figure 4 show remarkable similarity, despite substantial differences in specimen size and type, and provide further evidence that these sponge-like morphologies are structurally related. If the diverse specimens examined here are approximated as elastic solids,[30] then κ and κ' can both be related to the same elastic tensile modulus, and are therefore coupled so that $\kappa' = -\kappa(1-\nu)$, where ν denotes Poisson's ratio. Since ν is typically equal to 1/2, κ' reduces to $-\kappa/2$, and the bending energy density (ϕ) can be written as $\phi = \kappa(2\langle H\rangle^2 - \langle K\rangle/2)\Sigma$. A dimensionless bending energy corresponding to the characteristic volume element L^3 can thus be evaluated according to $\phi/\kappa = (2\langle H\rangle^2 - \langle K\rangle/2)\Sigma L^3$. Computed values of ϕ/κ are 13.3 ± 2.2 for all three polymeric systems and the strut-like TB_3. Slightly smaller values of ϕ/κ are obtained for the layered bone specimens (2.91 for TB_1 and 1.71 for TB_2). Within the level of approximation made here, the modest variation in these dimensionless energies, calculated from several independent measurements for systems differing substantially in material type and size, and the striking similarity of the curvature distributions in Figure 4 together provide strong evidence that a common mechanism governs complex morphological development.[26]

By skeletonizing 3D images such as those displayed in Figure 1, the number of channels per junction (N_c), as well as the average number of junctions (n_j) occupying L^3, can be extracted. The probabilities associated with N_c, as well as measured values of n_j, are listed in Table 1, and indicate surprisingly comparable structural connectivity. Values of the Euler–Poincaré characteristic and genus (g) measured directly from skeletonized 3D images are also provided in Table 1, and reveal that the polymer morphologies are all topologically equivalent, with g ranging from 2.10 to 2.36. Values of χ and g discerned from the TB specimens, however, exhibit more variability and generally less topological complexity (smaller g values) than the polymer morphologies. Values of χ and g estimated from the Gauss–Bonnet theorem of differential geometry (χ_{GB} and g_{GB}, respectively) are included in Table 1, and agree reasonably well with those measured directly from skeletonized 3D images, indicating that these sponge-like morphologies most likely represent closed surfaces of comparable topological complexity. In contrast, the gyroid morphology possesses a much larger g (7.1 from TEMT data and 9.0 from model predictions),[23] which signifies a more highly ordered nanostructure. While χ (or, alternatively, g) does not generally correlate with any of the local topological (i.e., curvature) measurements reported here, χ_{GB} (or g_{GB}) increases systematically with increasing ϕ/κ, suggesting that bending energy may be related to global topology.

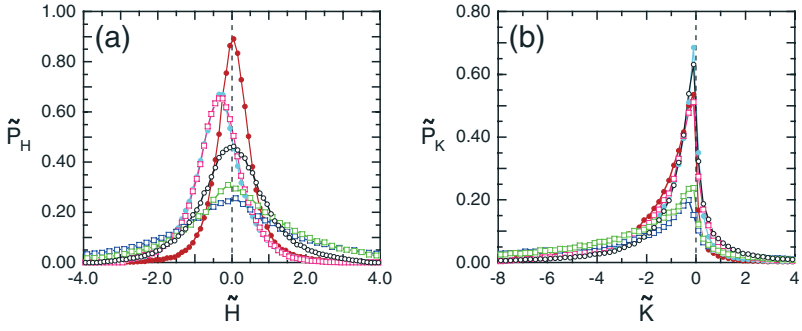

Fig. 4. Scaled probability densities of the a) mean ($\tilde{H}$) and b) Gaussian ($\tilde{K}$) curvatures measured from the sponge-like bicontinuous morphologies examined here (the symbols are the same as those used in Fig. 3). These scaled probability densities are given by $\tilde{P}_H(\tilde{H}) = P_H(H)\Sigma$ and $\tilde{P}_K(\tilde{K}) = P_K(K)\Sigma^2$, where $\tilde{H} = H/\Sigma$, $\tilde{K} = K/\Sigma^2$ and Σ denotes the interfacial area/volume. Measured values of Σ are provided in Table 1. The positions corresponding to $\tilde{H} = 0$ in (a) and $\tilde{K} = 0$ in (b) are denoted by dashed lines, and the solid lines serve to connect the data.

The results reported here, measured directly from 3D images, confirm that sponge-like bicontinuous morphologies exhibit structural similarities despite significant differences in size scale and material type. This conclusion,

  0935-9648/02/2211-1617 $ 17.50+.50/0

ADVANCED MATERIALS

coupled with the classification paradigms described herein, can be used to facilitate the systematic design of soft materials for applications requiring structural bicontinuity. One such example is the development of biocomposite materials,[31] such as iliac bone transplants coated with biodegradable polymer. If the polymer possesses a sponge-like morphology of specific length scale and classification, it may expedite bone regeneration through directed growth. Directed growth can, in principle, be extended to other biological systems, in which case bicontinuous materials could serve as biomimetic scaffolding media at targeted length scales. Nanoporous inorganic materials derived from organic templates for separation, microelectronics, and catalysis technologies constitute another use of bicontinuous media under serious consideration.[6,7,20] Parameters such as permeability coefficients and sorption isotherms describe the efficacy of these technologies, and must be related to material morphology for design and quality-control purposes.[4] The curvature and topological characteristics provided here constitute unambiguous metrics to which thermodynamic, transport, or mechanical properties can be directly related, and may be readily extended to multifunctional hybrid or self-organized materials containing particulate[32] or fibrillar[33] networks.

Experimental

The BC is a poly[styrene–*b*–(styrene–*r*–isoprene)–*b*–isoprene] triblock copolymer with a number-average molecular weight ($\overline{M}_n$) of 160 kg mol^{-1} and an overall composition of 50 wt.-% styrene. This BC is mixed with polystyrene (PS, $\overline{M}_n$ = 20 kg mol^{-1}) to form a 20:80 BC/PS (by weight) blend. Details regarding image acquisition by TEMT are provided elsewhere [18]. The SD polymer blends are composed of polybutadiene (PB) and deuterated polybutadiene (DPB) with $\overline{M}_n$ values of 89 and 127 kg mol^{-1}, respectively. Two blends, one designated SD_1 with 38:62 DPB/PB (by volume) and the other denoted SD_2 with 48:52 DPB/PB (by volume), are homogenized and then annealed at 40 °C for 2943 and 1673 min, respectively, to induce late-stage SD. The conditions under which LSCM was performed have been previously described [26]. Iliac bone specimens exhibiting layered (TB_1 and TB_2) and strut-like (TB_3) morphologies have been obtained from 60-, 64-, and 61-year-old women, respectively, with hip osteoarthrosis. The μCT conditions used to collect these images are discussed elsewhere [27].

Received: May 28, 2002

[1] L. E. Scriven, *Nature* **1976**, *263*, 123.
[2] S. Hyde, S. Andersson, K. Larsson, Z. Blum, T. Landh, S. Lidin, B. W. Ninham, *The Language of Shape*, Elsevier Science B.V., Amsterdam **1997**.
[3] R. H. Templer, *Curr. Opin. Colloid Interface Sci*. **1998**, *3*, 255.
[4] A commercial separations column based on a bicontinuous silica microstructure [H. Jinnai, K. Nakanishi, Y. Nishikawa, J. Yamanaka, T. Hashimoto, *Langmuir* **2001**, *17*, 619] has been found to outperform conventional packed bead columns.
[5] M. W. Matsen, F. S. Bates, *J. Chem. Phys.* **1997**, *106*, 2436.
[6] Y. H. Sakamoto, M. Kaneda, O. Terasaki, D. Y. Zhao, J. M. Kim, G. Stucky, H. J. Shim, R. Ryoo, *Nature* **2000**, *408*, 449.
[7] A. C. Finnefrock, R. Ulrich, A. Du Chesne, C. C. Honeker, K. Schumacher, K. K. Unger, S. M. Gruner, U. Wiesner, *Angew. Chem. Int. Ed.* **2001**, *40*, 1208.
[8] R. Strey, W. Jahn, G. Porte, P. Bassereau, *Langmuir* **1990**, *6*, 1635.
[9] H. Hoffmann, C. Thunig, U. Munkert, H. W. Meyer, W. Richter, *Langmuir* **1992**, *8*, 2629.
[10] B. M. Discher, Y. Y. Won, D. S. Ege, J. C. M. Lee, F. S. Bates, D. E. Discher, D. A. Hammer, *Science* **1999**, *284*, 1143.
[11] F. S. Bates, G. H. Fredrickson, *Phys. Today* **1999**, *52*, 32.
[12] S. Förster, B. Berton, H. P. Hentze, E. Kramer, M. Antonietti, P. Lindner, *Macromolecules* **2001**, *34*, 4610.
[13] D. A. Hajduk, P. E. Harper, S. M. Gruner, C. C. Honeker, G. Kim, E. L. Thomas, L. J. Fetters, *Macromolecules* **1994**, *27*, 4063.
[14] M. F. Schulz, F. S. Bates, K. Almdal, K. Mortensen, *Phys. Rev. Lett.* **1994**, *73*, 86.
[15] J. H. Laurer, D. A. Hajduk, J. C. Fung, J. W. Sedat, S. D. Smith, S. M. Gruner, D. A. Agard, R. J. Spontak, *Macromolecules* **1997**, *30*, 3938.
[16] L. Zhu, P. Huang, S. Z. D. Cheng, Q. Ge, R. P. Quirk, E. L. Thomas, B. Lotz, J. C. Wittmann, B. S. Hsiao, F. J. Yeh, L. Z. Liu, *Phys. Rev. Lett.* **2001**, *86*, 6030.
[17] E. Hecht, K. Mortensen, H. Hoffmann, *Macromolecules* **1995**, *28*, 5465.
[18] J. H. Laurer, J. C. Fung, J. W. Sedat, S. D. Smith, J. Samseth, K. Mortensen, D. A. Agard, R. J. Spontak, *Langmuir* **1997**, *13*, 2177.
[19] F. S. Bates, W. W. Maurer, P. M. Lipic, M. A. Hillmyer, K. Almdal, K. Mortensen, G. H. Fredrickson, T. P. Lodge, *Phys. Rev. Lett.* **1997**, *79*, 849.
[20] P. D. Yang, D. Y. Zhao, D. I. Margolese, B. F. Chmelka, G. D. Stucky, *Nature* **1998**, *396*, 152.
[21] E. L. Thomas, D. M. Anderson, C S. Henkee, D. Hoffman, *Nature* **1988**, *334*, 598.
[22] H. Jinnai, Y. Nishikawa, R. J. Spontak, S. D. Smith, D. A. Agard, T. Hashimoto, *Phys. Rev. Lett.* **2000**, *84*, 518.
[23] H. Jinnai, T. Kajihara, H. Watashiba, Y. Nishikawa, R. J. Spontak, *Phys. Rev. E* **2001**, *64*, 10 803.
[24] M. E. Cates, *Philos. Trans. R. Soc. London, Ser. A* **1993**, *344*, 339.
[25] M. Fialkowski, A. Aksimentiev, R. Holyst, *Phys. Rev. Lett*. **2001**, *86*, 240.
[26] H. Jinnai, T. Koga, Y. Nishikawa, T. Hashimoto, S. T. Hyde, *Phys. Rev. Lett.* **1997**, *78*, 2248.
[27] M. Ito, T. Nakamura, T. Matsumoto, K. Tsurusaki, K. Hayashi, *Bone (N.Y., NY, U.S.)* **1998**, *23*, 163.
[28] A. G. Evans, *MRS Bull*. **2001**, *26*, 790.
[29] H. Jinnai, H. Watashiba, T. Kajihara, Y. Nishikawa, M. Takahashi, M. Ito, *Bone (N.Y., NY, U.S.)* **2002**, *30*, 191.
[30] A. Fogden, S. T. Hyde, G. Lundberg, *J. Chem. Soc., Faraday Trans.* **1991**, *87*, 949.
[31] L. A. Estroff, A. D. Hamilton, *Chem. Mater.* **2001**, *13*, 3227.
[32] T. C. Merkel, B. D. Freeman, R. J. Spontak, Z. He, I. Pinnau, P. Meakin, A. J. Hill, *Science* **2002**, *296*, 519.
[33] X. Y. Liu, P. D. Sawant, *Adv. Mater*. **2002**, *14*, 421.

Monodisperse Diameter-Modulated Gold Microwires

By *Sven Matthias*, *Jorg Schilling*, *Kornelius Nielsch*, *Frank Müller*, *Ralph B. Wehrspohn*,* and *Ulrich Gösele*

Recently, considerable interest has grown in the use of monodisperse metallic nano- and microwires in applications such as surface-enhanced Raman spectroscopy (SERS),[1] metallo-dielectric photonic crystals,[2] perpendicular magnetic storage,[3] and selective thermal emitters.[4] Furthermore, microwires with diameters of ca. 1 μm, consisting of periodically varying metals with different reflectivity such as silver and gold, have been shown to be useful as barcodes in biodiagnostics.[5] In principle, the same effect of differential reflectivity could be obtained if the wire diameter varied periodically, or even non-periodically, via a controlled process. The pore diameter of macroporous silicon can be varied during the growth of the pores.[6–8] Currently, these structures are used as three-dimensional photonic crystals[9] or possibly particle separating filters.[10] However, using those pore arrays as a template would yield modulated microwires. In this paper, we will focus on the fabrication and characterization of monodis-

[*] Dr. R. B. Wehrspohn, S. Matthias, Dr. J. Schilling, Dr. K. Nielsch, Dr. F. Müller, Prof. U. Gösele
Max-Planck-Institute of Microstructure Physics
Weinberg 2, D-06120 Halle (Germany)
E-mail: wehrspoh@mpi-halle.de

  0935-9648/02/2211-1618 $ 17.50+.50/0